Frontiers in Bioscience Landmark

Front. Biosci. (Landmark Ed) **2026**; 31(10): 49650
https://doi.org/10.31083/FBL49650

Original Research

RAMP1 Promotes Lymphatic Metastasis in Head and Neck Squamous Cell Carcinoma via *VEGF-C/PROX-1* Mediated Lymphangiogenesis

Xiaohua Luo[1,2], Yanshi Li[1], Tongling Wen[1], Lin Chen[1], Huixi Wang[2], Tao Lu[1], Zhihai Wang[1], Chuan Liu[1], Min Wang[1], Mengna Wang[1], Zhaobo Cheng[1], Min Pan[1], Guohua Hu[1,*]

[1]Department of Otorhinolaryngology, The First Affiliated Hospital of Chongqing Medical University, 400016 Chongqing, China
[2]Department of Otorhinolaryngology, Chongqing University Fuling Hospital, 408000 Chongqing, China
*Correspondence: 2h4841@hospital.cqmu.edu.cn (Guohua Hu)
Academic Editor: Amancio Carnero Moya
Submitted: 2 January 2026 Revised: 20 April 2026 Accepted: 30 April 2026 Published: 30 September 2026

Abstract

Background: Lymph node metastasis (LM) is associated with poor prognosis in head and neck squamous cell carcinoma (HNSCC); however, the molecular drivers of tumor-induced lymphangiogenesis remain incompletely understood. **Methods:** This study aimed to analyze clinical HNSCC specimens using transcriptomic sequencing to identify differentially expressed genes associated with lymphatic metastasis. Receptor Activity-Modifying Protein 1 (RAMP1) expression was quantified by reverse transcription-quantitative polymerase chain reaction (RT-PCR), immunohistochemistry, and Western blotting. Moreover, functional assays (Transwell, wound healing, Cell Counting Kit-8 (CCK-8), and tube formation) were performed using HNSCC cell lines and human lymphatic endothelial cells. Furthermore, a footpad xenograft mouse model was established to investigate the effects of RAMP1 on tumor growth, lymphangiogenesis, and LM *in vivo*. **Results:** *RAMP1* was significantly overexpressed in HNSCC tissues with LM. Elevated *RAMP1* expression was associated with poor prognosis, increased intratumoral lymphatic vessel density ($p < 0.05$), and strong predictive power for LM (area under the curve (AUC) = 0.808). *In vitro*, *RAMP1* knockdown reduced proliferation, migration, and invasion of HNSCC cells, and decreased expression of the lymphangiogenic factor vascular endothelial growth factor C (*VEGF-C*) and its transcriptional regulator Prospero homeobox protein 1 (*PROX-1*). Conversely, *RAMP1* overexpression had opposite effects. *RAMP1* also promoted tube formation in lymphatic endothelial cells through a paracrine mechanism. *In vivo*, *RAMP1* overexpression increased lymphangiogenesis and LM in xenograft models, whereas its suppression showed inhibitory effects ($p < 0.05$). **Conclusions:** This study indicated that *RAMP1* promotes lymphangiogenesis and lymphatic metastasis in HNSCC by regulating the *VEGF-C/PROX-1* signaling axis, thereby identifying *RAMP1* as a potential pro-metastatic factor and therapeutic target for HNSCC.

Keywords: squamous cell carcinoma of head and neck; receptor activity-modifying protein 1; lymphatic metastasis; lymphangiogenesis; vascular endothelial growth factor C; PROX-1

1. Introduction

Head and neck squamous cell carcinoma (HNSCC) is a common malignancy with a gradually increasing prevalence globally. It originates from the mucosal epithelial tissues of the oral cavity, larynx, and pharynx. Despite advances in diagnosis and treatment strategies, the prognosis of HNSCC remains poor, with relatively low five-year survival rates [1,2,3]. Lymph node metastases are an important prognostic factor associated with poor survival [4,5]. The occurrence of metastasis, particularly in multiple lymph nodes or extracapsular extension, significantly reduces patient survival and complicates treatment, highlighting the importance of understanding the underlying mechanisms [6]. Lymph node metastasis (LM) is a complex process involving multiple steps, including detachment of tumor cells, their infiltration into adjacent lymphatic vessels, migration through the lymphatic system, and eventual colonization and proliferation within lymph nodes [7]. A key component of this process is tumor-induced lymphangiogenesis, which establishes a structural pathway for tumor cells to detach from the original tumor and move to regional lymph nodes, while also actively influencing tumor growth by secreting chemokines and altering the immune microenvironment [8,9].

Recent studies have validated the fundamental regulatory roles of the vascular endothelial growth factor C (*VEGF-C*)/Vascular endothelial growth factor receptor 3 (*VEGFR3*) signaling pathway and the transcription factor Prospero homeobox protein 1 (*PROX-1*) in lymphangiogenesis [10,11,12,13]; however, the upstream regulatory mechanisms of lymphatic metastasis in HNSCC remain elusive, which limits the advancement of associated targeted therapeutic strategies [14]. Moreover, most studies focus on ligands and receptors in the lymphatic signaling cascade or on the modulation of lymphangiogenesis by specific growth factors; however, alternative regulatory molecules have not been comprehensively studied [15,16]. There-

Copyright: © 2026 The Author(s). Published by IMR Press.
This is an open access article under the CC BY 4.0 license.

Publisher's Note: IMR Press stays neutral with regard to jurisdictional claims in published maps and institutional affiliations.

fore, the screening and identification of novel regulatory molecules involved in lymphangiogenesis in HNSCC, as well as their mechanisms of action, are scientifically and clinically important for enhancing the molecular regulatory network of lymphatic metastasis in HNSCC and for the development of new diagnostic and therapeutic strategies.

Receptor Activity-Modifying Protein 1 (RAMP1) is a single-pass transmembrane protein that is a crucial auxiliary component of G protein-coupled receptors (GPCRs), particularly the calcitonin gene-related peptide (CGRP) receptor complex. The extracellular N-terminal domain of RAMP1 binds to the calcitonin receptor-like receptor (CLR), enabling the formation of a high-affinity CGRP receptor [17,18,19]. This association is crucial for regulating numerous physiological and pathological processes, such as neurotransmission, vasomotor function, and inflammatory responses [20,21]. Emerging evidence indicates that *RAMP1* is involved in tumor biology. In gastric cancer, the *CGRP–RAMP1* axis promotes tumor progression by activating *MAPK* and *PI3K* signaling pathways [22]. In prostate cancer, *RAMP1* promotes cell cycle progression and inhibits apoptosis [23]. In Ewing sarcoma, targeting the *CALCB/RAMP1* axis suppresses tumor growth [24]. Furthermore, *RAMP1* has been associated with lymphangiogenesis, as its silencing impairs lymphatic vessel regeneration in models of inflammation and tissue repair [25,26,27]. However, despite these findings, certain knowledge gaps remain. For instance, the role of *RAMP1* in HNSCC, particularly LM, has not been investigated. It is also unclear whether *RAMP1* contributes to tumor-induced lymphangiogenesis and subsequent lymphatic dissemination in HNSCC. Furthermore, the relationship between *RAMP1* and the *VEGF-C/PROX-1* signaling axis has not been defined. Thus, the molecular mechanisms by which *RAMP1* may regulate lymphatic metastasis in HNSCC remain to be elucidated.

Therefore, this study integrated multi-omics analysis, molecular biology techniques, and animal models to comprehensively investigate the regulatory function of *RAMP1* in HNSCC-related lymphangiogenesis and metastasis. Furthermore, clinical samples were analyzed to determine *RAMP1*'s expression patterns and association with clinical outcomes. Moreover, cellular functional assays and *in vivo* analyses were carried out to assess the molecular mechanisms underlying *RAMP1*'s effect on HNSCC lymphangiogenesis and lymphatic dissemination. This study aims to provide novel insights and identify potential therapeutic targets for HNSCC.

2. Materials and Methods

2.1 Clinical Specimens

This investigation enrolled 137 HNSCC patients who underwent surgical treatment at Fuling Hospital, an affiliated hospital of Chongqing University between 2016 and 2024. All cases were retrospectively analyzed according to the eighth edition of the American Joint Committee on Cancer (AJCC) staging system, which was applied uniformly across the cohort to ensure consistency. Clinical and pathological data were independently reviewed and reclassified by the same team of head and neck surgeons and pathologists to reduce potential bias associated with the extended enrollment period. These participants had not undergone neoadjuvant chemotherapy, radiotherapy, or any other antitumor treatment before their surgical procedures. During the surgery, the tumor and its adjacent normal tissues (from areas >5 cm from the tumor margin) were sampled.

Inclusion criteria were: (1) Patient with HNSCC diagnosis confirmed by postoperative pathological examination; (2) Patients who completed preoperative imaging examinations, including neck ultrasound, contrast-enhanced CT, or MRI, to determine tumor stage and lymph node status; (3) Patients who had complete clinical data and follow-up records; and (4) Patients with first-time laryngeal or pharyngeal resection without surgical contraindications.

Exclusion criteria were: (1) Individuals with a history of antitumor treatment, including radiotherapy and chemotherapy, before surgery; (2) Individuals with concurrent presence of other malignant tumors; and (3) those with the presence of distant metastasis.

In total, 137 HNSCC patients with complete clinical data met the criteria and were included in the study. Their baseline clinical characteristics are detailed in Table 1. Tissue samples were collected from 77 of 137 patients. Written informed consent was obtained from all patients or their legal guardians prior to enrollment. Furthermore, this investigation was approved by the Ethics Committee at Chongqing University Fuling Hospital and was conducted in accordance with the Declaration of Helsinki.

2.2 RNA Isolation and qRT-PCR

Total RNA from 16 freshly-frozen HNSCC tissues was isolated using an RNA extraction kit (Takara, No9767, Dalian, China). Of the 16 specimens, only 8 indicated LM. To ensure RNA integrity, its purity was assessed by measuring the A260/A280 ratio, with acceptable values between 1.8 and 2.0. The acquired RNA was then quantified via a Nanodrop Nucleic Acid Quantifier. The PrimeScript RT reagent kit (Takara, CN830A, Dalian, China) was utilized for reverse transcription as directed. qRT-PCR was performed according to the protocol provided with the SYBR® Green kit (Takara). GAPDH was set as an endogenous reference, and the relative RAMP1 mRNA expression level was calculated via the method of $2^{-\Delta\Delta Ct}$. The experiment was repeated thrice, and each sample was assayed in triplicate wells. Primer sequences employed were:

RAMP1-F: 5′-GGAGGCTAACTACGGTGCC-3′
RAMP1-R: 5′-CTCCCTGTAGCTCCTGATGG-3′
GAPDH-F: 5′-CAGCGACACCCACTCCTC-3′
GAPDH-R: 5′-TGAGGTCCACCACCCTGT-3′

IMR Press

Table 1. Clinicopathological features of HNSCC patients.

Characteristic	Category	Cases (%)
Gender	Male	134 (97.8%)
	Female	3 (2.2%)
Age	<60	47 (34.3%)
	≥60	90 (65.7%)
Smoking	Yes	125 (91.2%)
	No	12 (8.8%)
T stage	Early (T1–T2)	99 (72.3%)
	Advanced (T3–T4)	38 (27.7%)
Lymphatic metastasis	Yes	61 (44.5%)
	No	76 (55.5%)
Pathological differentiation	Well/Moderately differentiated	127 (92.7%)
	poorly differentiated	10 (7.3%)

HNSCC, head and neck squamous cell carcinoma.

2.3 Protein Extraction and Western Blotting

Whole protein was isolated from 16 HNSCC tissue samples (8 samples with LM and 8 samples without LM) and their adjacent normal tissues, using a kit (KeyGen BioTECH, China). The proteins were isolated on 12% SDS-PAGE via electrophoresis and transferred onto polyvinylidene difluoride (PVDF) membranes, which were then occluded for an hour, and were then treated overnight with primary antibodies against RAMP1 (Abcam, ab156575, UK, diluted 1:1000), VEGF-C (Abcam, ab9546, UK, diluted 1:1000), LYVE-1 (Abcam, ab219556, diluted 1:1000), SOX2 (Proteintech, 66411, China, diluted 1:1000), PROX-1 (Abcam, ab199359, diluted 1:1000), and GAPDH (Abcam, ab181602, diluted 1:1000) at 4 °C. Then, the membranes were probed with an anti-rabbit secondary antibody (diluted to 1:2000; Beyotime, China) at ambient temperature for 2 hours. The protein bands were detected using an ECL kit (Beyotime) and visualized on a ChemiDoc Touch Imaging System (Bio-Rad, USA).

2.4 Immunohistochemistry (IHC) Analysis

This assay was carried out by following the standard protocol. Briefly, the samples were deparaffinized with xylene twice, each for 10 minutes, rehydrated using serially graded alcohol solutions (100, 95, 85, and 75%; for 5 minutes at each concentration), and rinsed with phosphate-buffered saline (PBS) 3 times (each for 5 minutes). Then, endogenous peroxidase activity was inhibited by treating the specimens with 3% hydrogen peroxide for 15 minutes at ambient temperature, washing them three times in PBS for 5 minutes each, and subjecting them to a high-temperature, high-pressure citrate buffer treatment at pH 6.0 to retrieve the antigen. The samples were then cooled to ambient temperature, rinsed three times with PBS (5 min/rinse), treated with blocking solution for 30 min at ambient temperature, and probed with primary antibodies against RAMP1 (Abcam, ab203282, 1:500 dilution) and LYVE-1 (Abcam, ab33682, 1:200 dilution) at 4 °C for 24 hours. Next, the samples were PBS-washed 3 times (5 minutes/wash), exposed to Boost IHC Detection Reagent (ZSGB-BIO, China) for 20 min at 37 °C, rinsed 3 times, and reacted with diaminobenzidine (DAB) solution for 5 min for color development, which was observed under a microscope. The reaction was halted by the addition of distilled water. The samples were then stained with hematoxylin for 30 seconds, differentiated with HCl/alcohol for 3 seconds, blued using ammonia water for 30 seconds, dehydrated through a sequential series of graded alcohols (75, 85, 95, and 100%, each for 5 min), cleared in xylene (I and II, each for 10 min), and lastly mounted with neutral gum. Negative controls were treated identically, but instead of the primary antibody, PBS was used.

The IHC data were evaluated by two experienced pathologists blinded to group assignment. Inter-observer agreement between the two pathologists was assessed using Cohen's kappa coefficient based on 20 randomly selected samples. The kappa value was 0.82 (95% CI: 0.74–0.90), which was almost perfect. In cases of disagreement, a final score was determined by consensus review using a multihead microscope. Then the staining intensity was scored, and the percentage of positive cells was calculated. The staining intensity scores were: 0 = no staining; 1 = light yellow; 2 = light brown; and 3 = dark brown. Furthermore, positively stained cells were scored as follows: 0 = 0–5%, 1 = 5–25%, 2 = 25–50%, 3 = 50–75%, and 4 = 75–100%. The overall score was determined by multiplying the intensity score by the percentage score. A final score of 0 = negative (–), 1–4 = weakly positive (+), 5–8 = positive (++), and 9–12 = strongly positive (+++). Low expression was indicated by scores <5, while scores ≥5 indicated high expression [28].

Micro-lymphatic vessel density (MLVD) was detected using LYVE-1, a specific lymphatic endothelial cell marker, which showed brownish-yellow staining. Under 100× magnification, 2 regions with the highest MLVD (hotspots) were visualized. Then, under 200× magnifica-

tion, 5 random fields within each hotspot were selected for counting micro-lymphatic vessels. For each sample, the MLVD value was assessed by averaging the counts from these 10 fields [29].

2.5 Analysis of Clinical Prognostic Value

Based on IHC levels of RAMP1, cases were categorized into high- and low-expression cohorts. Furthermore, the differences in overall survival (OS) between the two cohorts were examined by the Log-rank test. Kaplan-Meier curves assessed survival. Independent risk factors influencing HNSCC prognosis were examined using univariate and multivariate Cox proportional hazards regression analyses.

2.6 Cell Culture

This investigation acquired the following HNSCC cell lines from the Center for Molecular and Cell Science at the Chinese Academy of Sciences (Shanghai, China): CAL27 (oral squamous cell carcinoma), HPV-negative FADU (hypopharyngeal squamous cell carcinoma), HPV-positive UM-SCC47 (tonsil squamous cell carcinoma), and SCC15 (tongue squamous cell carcinoma). Cells were propagated in 1% penicillin/streptomycin (Beyotime, China) and 10% fetal bovine serum (FBS; Gibco, USA) in DMEM (Gibco) at 37 °C in 5% CO_2. The culture medium was replaced routinely. Cells were passaged at 80–90% confluence using 0.25% trypsin–EDTA. Short tandem repeat (STR) profiling was employed for cell line identity, and all cultures were regularly tested for mycoplasma contamination using the MycoAlert™ Mycoplasma Detection Kit (Lonza, Switzerland) in accordance with the manufacturer's instructions. Testing was performed before experimental use and at regular intervals (approximately monthly) during maintenance. Only cells in the logarithmic growth phase were used for all experiments.

2.7 Lentiviral Transduction

To establish stable cell models with RAMP1 knockdown (KD) or overexpression (OE), specific shRNA sequences targeting *RAMP1* as well as RAMP1 OE fragments were designed, synthesized, and cloned into lentiviral vectors (Ubi-MCS-firefly_luciferase-IRES-Puromycin; acquired from Genechem, Shanghai, China). The experiment included four groups: sh-RAMP1 (RAMP1 KD), vector (OE negative control), sh-NC (KD negative control), and OE-RAMP1 (RAMP1 OE). All cell lines (5×10^5/well) were grown in 6-well plates until 50–60% confluent. Then, transduction was performed. Based on pre-optimized conditions, lentiviral particles were added to each well at a multiplicity of infection (MOI) of 10. To enhance transduction efficiency, 5 µg/mL of polybrene was added. After 6 hours, fresh DMEM containing 10% FBS was added, and the cells were cultured for another 48 hours. Subsequently, the medium was replaced with a selection medium containing puromycin (2 µg/mL). Positive cells were isolated by continuing the culture until all cells in the negative control groups had perished, yielding stably transduced cell populations. Finally, the RAMP1 KD or OE efficiency was evaluated via qRT-PCR and Western blot analyses. The cell line with the highest transduction efficiency was selected for further experiments.

2.8 CCK-8 Proliferation Assay

Stably transduced FADU and SCC15 cells (2000/well) were grown in 96-well plates, with each well comprising 100 µL of 10% FBS containing DMEM for 12 hours at 37 °C in 5% CO_2. At 0, 24, 48, 72, and 96 hours post-incubation, 10 µL of CCK-8 reagent (without FBS) was added to each well for 2 hours, and the absorbances at 450 nm were read in a microplate reader to assess cell proliferation activity. Each group was assayed thrice, with three replicates. Cell proliferation was determined relative to the absorbance at 0 hours.

2.9 Wound Healing Assay

Stably transduced FADU and SCC15 cells (5×10^5/well) were grown in 6-well plates in 10% FBS containing DMEM until 100% confluent. Then, a sterile pipette tip was used to scrape the cell monolayer 3–5 times in parallel to create a wound, ensuring a uniform width for each scratch. Cells were then rinsed 3 times with PBS to remove dislodged cell debris, cultured in serum-free DMEM, and monitored for scratch-healing rate at 0, 24, and 48 hours under inverted microscopy. ImageJ was employed to measure scratch width. Wound closure rates were determined as follows: (Initial scratch width – Scratch width at a given time point) / Initial scratch width × 100%. Each group was evaluated thrice separately with replicates.

2.10 Invasion Assay

For cell invasion assays, Matrigel matrix (BD Biosciences, USA) was coated on Transwell chambers (24-well plate, 8 µm pore polycarbonate membrane, Corning, USA). Briefly, 50 µL of Matrigel in serum-free DMEM (1:8 ratio) was dispensed into each chamber at 37 °C in 5% CO_2 for 4 hours. Then, stably transduced FADU cells (5×10^4/100 µL of serum-free DMEM) were introduced into the top compartment, whereas 600 µL of 15% FBS-containing DMEM was added to the lower compartment as a chemoattractant. The plate was kept at 37 °C in 5% CO_2 for 24 hours. Non-invading cells in the membrane's upper surface were accurately removed while employing a cotton swab. The chambers were rinsed with PBS 3 times, preserved with 4% paraformaldehyde for 30 minutes, rinsed again with PBS 3 times, stained with a 0.5% crystal violet-methanol solution at ambient temperature for 15 minutes, and washed 3 times with PBS to remove excess stain. Cells on the bottom surface of the membrane were imaged and quantified via inverted microscopy from 5 randomly selected fields per chamber. Each group was analyzed independently three times, each time with 3 triplicate.

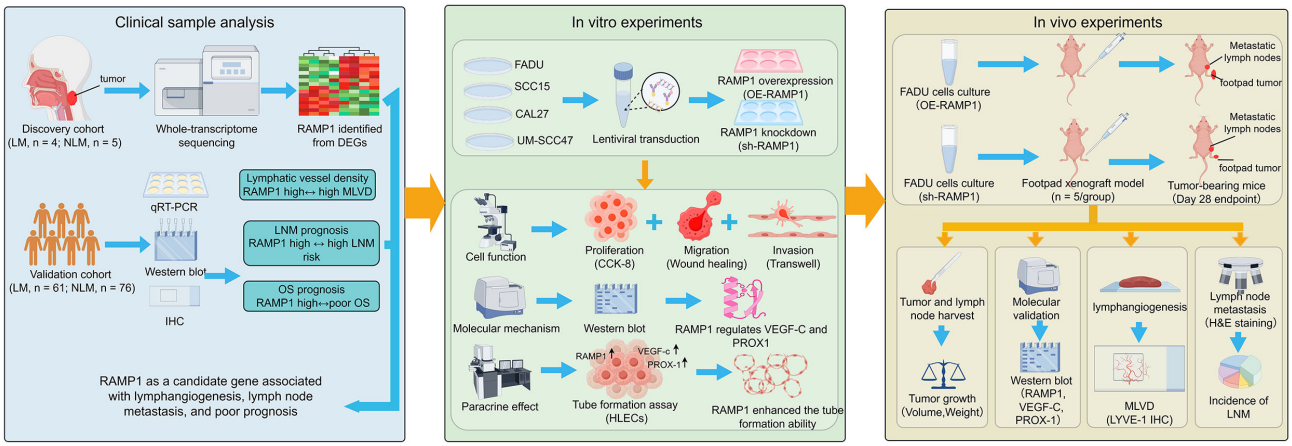

Fig. 1. Schematic overview of the study design. (A) Clinical sample analysis. A discovery cohort (LM, n = 4; NLM, n = 5) was subjected to whole-transcriptome sequencing, which revealed *RAMP1* as a differentially expressed gene. Validation was performed in a larger cohort by qRT-PCR, Western blot, and immunohistochemistry. RAMP1 high expression correlated with increased micro-lymphatic vessel density (MLVD). (B) *In vitro* experiments. *RAMP1* knockdown and overexpression in HNSCC cell lines (FADU, SCC15, CAL27, UM-SCC47) were established. Functional assays were conducted to evaluate proliferation, migration, and invasion. The expression of VEGF-C and PROX-1 was examined by Western blot. Conditioned media from RAMP1-modulated cells were used to evaluate tube formation in human lymphatic endothelial cells (HLECs). (C) *In vivo* experiments. A footpad xenograft model was established in BALB/c nude mice (n = 5 per group). After 28 days, tumor growth, lymphangiogenesis (LYVE-1 IHC), lymph node metastasis (H&E), and expression of RAMP1, VEGF-C, and PROX-1 were evaluated. LM, lymph node metastasis; NLM, no lymph node metastasis; *RAMP1*, Receptor Activity-Modifying Protein 1; qRT-PCR, quantitative real-time polymerase chain reaction; HNSCC, head and neck squamous cell carcinoma; *VEGF-C*, vascular endothelial growth factor C; *PROX-1*, Prospero homeobox protein 1.

2.11 Tube Formation Assay

For this assay, 50 µL of Matrigel/well was used to coat 96-well plates for an hour at 37 °C in 5% CO_2 to facilitate gel solidification. Then, human lymphatic endothelial cells (HLECs) in normal culture were digested by trypsin-EDTA and centrifuged to acquire a cell pellet, which was redissolved in conditioned medium collected from RAMP1 OE or KD FADU and SCC15 cells. Subsequently, 50 µL of a cell suspension (1×10^4 cells) was added to each well and incubated at 37 °C in 5% CO_2 for 24 hours. Then, 5 random fields from each well were imaged via inverted microscopy equipped with a 10× objective lens. The tube formation parameters, such as the number of junctions, cumulative tube length, and the number of mesh structures, were evaluated using the Angiogenesis Analyzer plugin in ImageJ (version 1.52v, National Institutes of Health, Bethesda, Maryland, USA). Each group was analyzed independently 3 times, each time with 3 triplicate.

2.12 Establishment of a Footpad Xenograft Mouse Model

BALB/c nude mice (five-week-old, male) were provided by Tengxin Biotechnology Co., Ltd. (Chongqing, China), and kept at the Animal Center of Chongqing Medical University under specific-pathogen-free (SPF) condition at 22–25 °C, in 50–60% humidity, in a 12-hour light/dark cycle, with unrestricted chow and water. The animals were acclimatized for a week before the experiments.

Stably transduced FADU cells (sh-NC, sh-RAMP1, vector, OE-RAMP1; 5×10^6 cells/mL) were resuspended in PBS, and 0.2 mL of this suspension, containing 1×10^6 cells, was subcutaneously injected into each mouse's right hind footpad (n = 5 mice/group). The animals' overall health and progression of footpad tumor growth were monitored daily. At 28 days post-injection, all animals were anesthetized by intraperitoneally injecting pentobarbital sodium (50 mg/kg). Deep anesthesia was confirmed by loss of pedal reflex, followed by euthanasia through cervical dislocation performed by trained personnel. Death was confirmed by the absence of respiration, heartbeat, and corneal reflex before tissue collection. Primary tumors in the popliteal lymph nodes and footpad were dissected and weighed. Moreover, tumor volume was evaluated as follows: Volume = (Length × Width^2) × π/6 [30].

Half of the tumor and lymph node tissue samples were used for qRT-PCR and Western blot analyses, while the remaining were preserved in 4% paraformaldehyde, embedded in paraffin, and used for IHC analysis. All *in vivo* assays were approved by the Animal Welfare and Ethics Committee of Chongqing University and followed the UK Animals (Scientific Procedures) Act and relevant guidelines from the National Institutes of Health. The study was carried out in accordance with the ARRIVE guidelines.

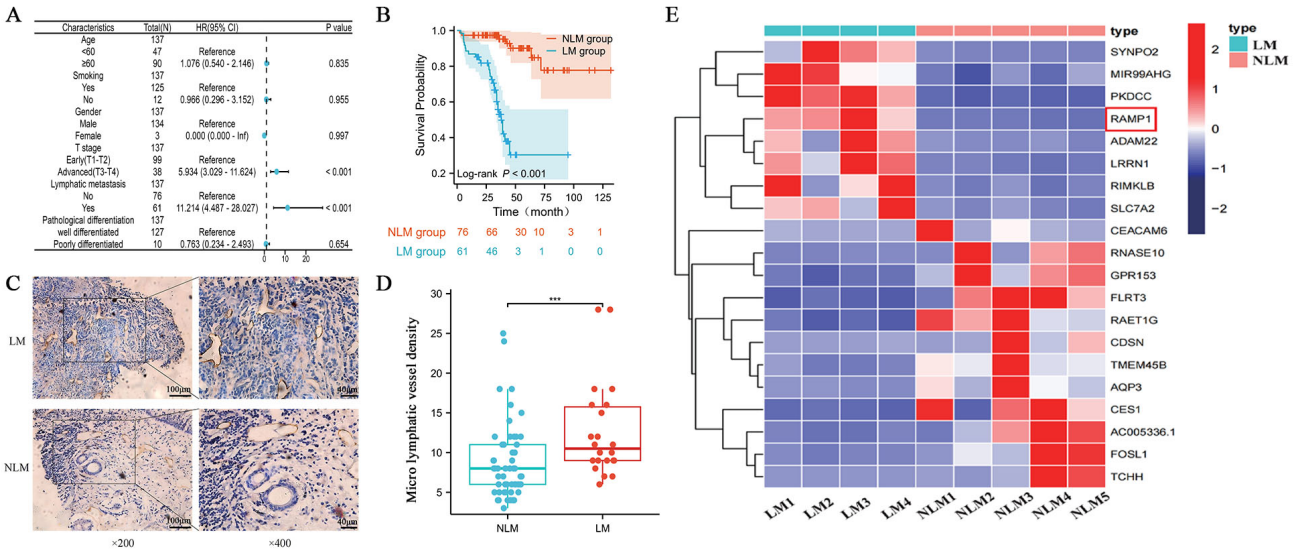

Fig. 2. In HNSCC patients, LM promotes poor prognosis through lymphangiogenesis. (A) Univariate Cox regression analysis of clinicopathological characteristics of 137 HNSCC patients. (B) Kaplan-Meier survival curves comparing patients with LM (LM group, n = 61) and no LM (NLM group, n = 76). (C) Representative IHC images of lymphatic vessels (LYVE-1 staining) in LM and NLM HNSCC tissues. Scale bar, 100 μm (200×) and 40 μm (400×), respectively. (D) MLVD quantification in 77 HNSCC tissues. The LM group exhibited substantially higher MLVD than the NLM group. (E) Heatmap of DEGs ($|\log_2 FC| > 1.5$, $p < 0.05$) between LM (n = 4) and NLM (n = 5) HNSCC tissues. RAMP1 was significantly up-regulated in metastatic tumors. The two-sided log-rank test was conducted for survival analysis in (B). Comparisons between two groups in (D) were analyzed using a two-tailed Student's *t*-test. DEGs in (E) were identified based on the criteria $|\log_2 FC| > 1.5$ and $p < 0.05$ (no multiple testing correction applied). ***$p < 0.001$.

2.13 Bioinformatics

Gene expression profiles (in TPM format) and clinical information of HNSCC cases were obtained from the TCGA database. The dataset comprised 566 samples (522 tumor specimens and 44 normal controls). The R package "TCGAbiolinks" (version 2.25.0) [PMID: 26704973] was employed for data extraction and preprocessing. Moreover, gene expression data related to HNSCC were also screened from the GEO GSE6631 dataset. This dataset comprised 44 samples, including 22 tumor and 22 normal samples. "GEOquery" in R was used to extract and normalize this dataset.

Furthermore, *RAMP1* expression across 33 cancer types in the TCGA database was assessed using TIMER2.0, facilitating a comprehensive pan-cancer analysis. KEGG pathway enrichment analyses and GO functional annotation for *RAMP1* and its associated genes were performed using "clusterProfiler" in R, with a significance threshold of $p < 0.05$.

2.14 Statistical Analysis

All data were statistically assessed with SPSS 22.0 and GraphPad Prism (version 8.0) and are presented as mean ± standard deviation (mean ± SD). Intergroup differences were evaluated using *t*-tests, and for the multigroup comparison, the one-way ANOVA followed by Tukey's test (if ANOVA revealed significant differences) was used. Categorical variables, such as the association between *RAMP1* expression and clinicopathological features, were analyzed using Pearson's χ^2 test. The correlation between *RAMP1* expression and MLVD, as well as between *RAMP1* expression and patient survival, was evaluated via Spearman's rank correlation and Kaplan-Meier curves, respectively, and their differences were assessed using the Log-rank test. A *p*-value < 0.05 depicted statistical significance. All experiments were conducted at least three times to ensure reliability.

3. Results

The overall study design is summarized in Fig. 1.

3.1 Lymphangiogenesis-Mediated LM Drives Poor Prognosis in HNSCC

Univariate Cox regression analysis of clinicopathological features in 137 HNSCC patients indicated that LM was strongly associated with poor prognosis (Fig. 2A). Furthermore, the multivariate Cox regression analysis revealed that LM serves as an independent prognostic factor influencing the OS of HNSCC (HR = 7.381, 95% CI = 2.770–19.667, $p < 0.001$) (Table 2). Moreover, Kaplan-Meier survival analysis showed that the OS of cervical LM patients was significantly reduced compared with the negative group (Fig. 2B).

Table 2. Univariate and multivariate Cox regression analyses of OS in HNSCC.

Characteristics	Univariate analysis		Multivariate analysis	
	HR (95% CI)	*p*-value	HR (95% CI)	*p*-value
Age				
<60	Reference			
≥60	1.076 (0.540–2.146)	0.835		
Smoking				
Yes	Reference			
No	0.966 (0.296–3.152)	0.955		
Gender				
Male	Reference			
Female	0.000 (0.000–Inf)	0.997		
T stage				
Early (T1–T2)	Reference		Reference	
Advanced (T3–T4)	5.934 (3.029–11.624)	<0.001	2.564 (1.251–5.255)	0.010
Lymphatic metastasis				
No	Reference		Reference	
Yes	11.214 (4.487–28.027)	<0.001	7.381 (2.770–19.667)	<0.001
Pathological differentiation				
Well/Moderately differentiated	Reference			
Poorly differentiated	0.763 (0.234–2.493)	0.654		

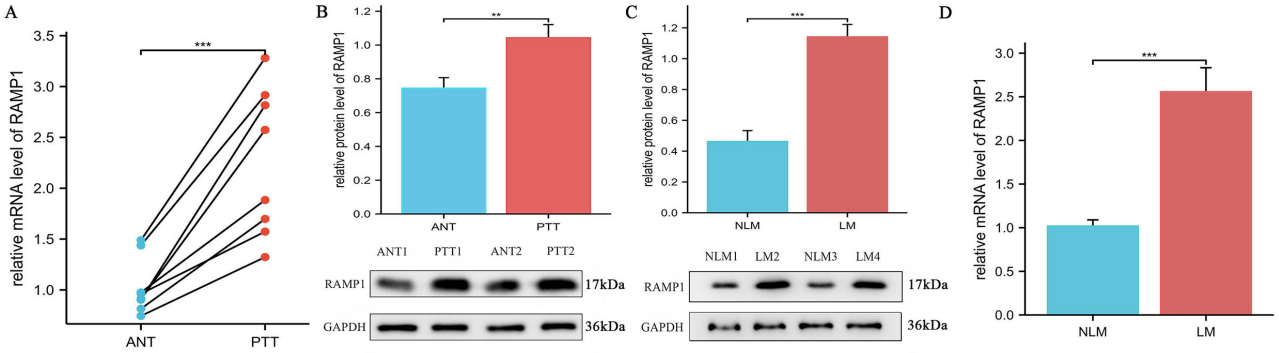

Fig. 3. *RAMP1* is up-regulated in HNSCC tissue and is linked with LM. (A) qRT-PCR measurement of *RAMP1* mRNA levels in 8 paired primary tumor tissues (PTT) and adjacent non-tumorous tissues (ANT). (B) Representative Western blot images (lower) and densitometric quantification of RAMP1 protein levels (upper) in PTT/ANT samples. (C) Representative Western blot images (lower) and densitometric quantification of RAMP1 protein levels (upper) in NLM/LM samples. (D) *RAMP1* mRNA levels in NLM and LM HNSCC tissues. All comparisons between two groups were analyzed via a two-tailed Student's *t*-test. Data are shown as mean ± SD. $^{**}p < 0.01$, $^{***}p < 0.001$.

To elucidate the relationship between lymphangiogenesis and LM, LYVE-1 IHC analysis was carried out on 77 HNSCC tumor samples to identify lymphatic vessels. It was found that the MLVD in HNSCC patients with cervical LM was significantly elevated relative to those without cervical LM ($p < 0.01$) (Fig. 2C,D). This suggests a significant correlation between lymphangiogenesis and cervical LM at the histopathological level in HNSCC. To identify pivotal genes regulating LM in HNSCC, transcriptomic analysis was conducted on tissue specimens from four individuals with cervical LM and five samples without LM. Based on the criterion of $|\log_2 FC| > 1.5$ and $p < 0.05$, several differentially expressed genes (DEGs) were successfully identified. Among them, *RAMP1* was substantially up-regulated in the LM-positive group (Fig. 2E).

3.2 RAMP1 Demonstrates Elevated Expression in HNSCC With LM and Correlates With Lymphangiogenesis and Adverse Prognosis

Western blotting and qRT-PCR analysis of 8 matched samples of HNSCC tumor tissues and adjacent normal tissue showed that RAMP1 protein and mRNA levels were significantly elevated in tumor specimens relative to their adjacent normal counterparts ($p < 0.05$) (Fig. 3A,B). Furthermore, *RAMP1* mRNA and protein expression of pri-

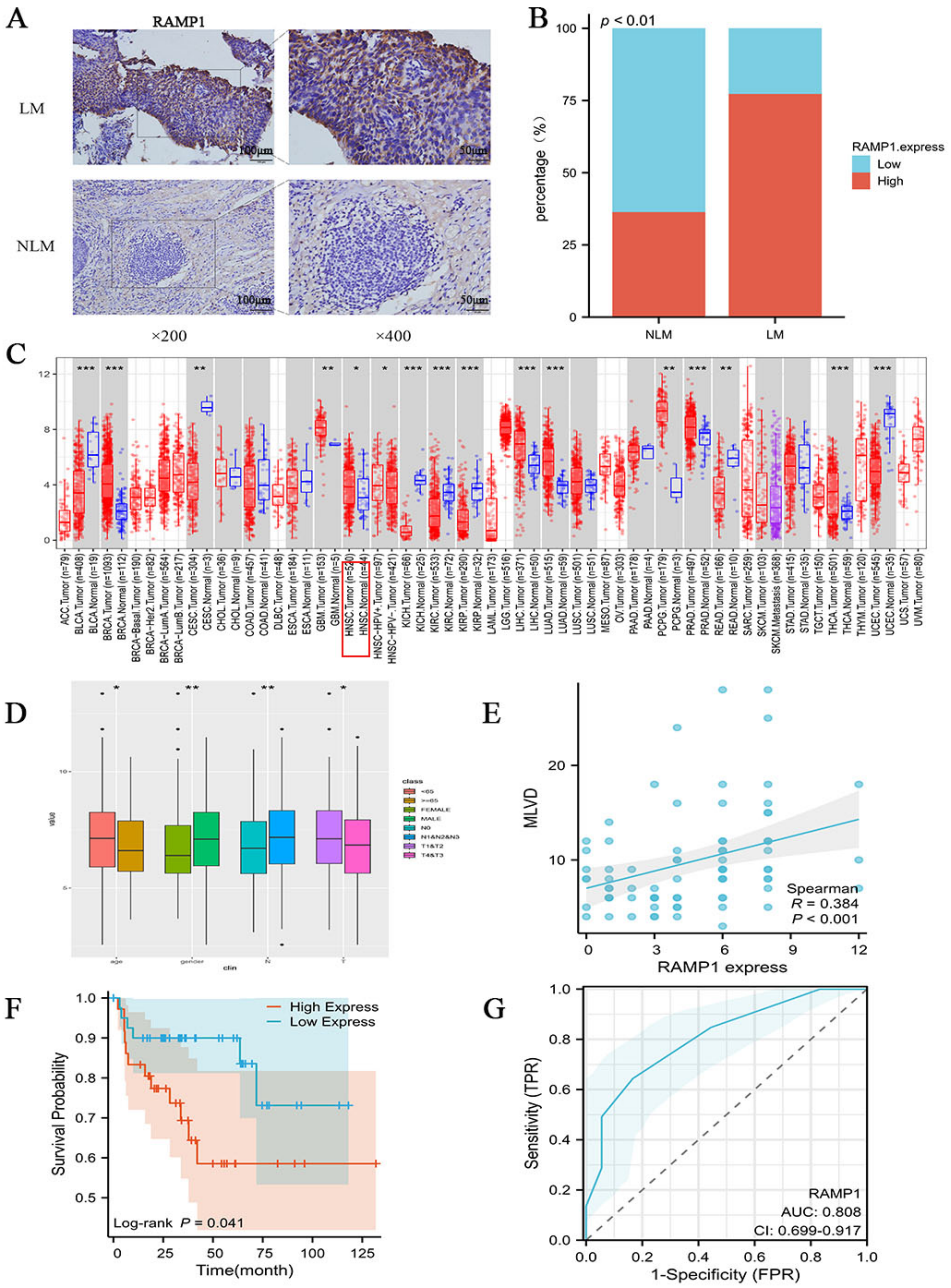

Fig. 4. Clinical and functional significance of *RAMP1* in HNSCC patients. (A) Representative IHC images of RAMP1 in LM and NLM HNSCC tissues. Scale bar: 100 μm (200×) and 50 μm (400×), respectively. (B) Percentage of tumors with high RAMP1 expression in NLM and LM cohorts. RAMP1 expression was categorized as high (IHC score ≥5) or low (IHC score <5) based on combined intensity and percentage scoring. The χ^2 test was used to compare the proportion of high RAMP1 expression between LM and NLM groups ($p < 0.05$). (C) Pan-cancer analysis of *RAMP1* expression across 33 cancer types using the TIMER2.0 database. (D) Elevated expression of *RAMP1* in LM HNSCC tissues from the TCGA-HNSC dataset (n = 522), stratified by age, sex, T classification, and N classification. A two-tailed Wilcoxon rank-sum test was performed to compare RAMP1 expression between LM and NLM groups. (E) Spearman correlations between RAMP1 IHC score and MLVD in 77 HNSCC tissues. (F) Kaplan-Meier survival curves of HNSCC patients stratified by RAMP1 expression. The optimal cut-off value (IHC score = 5) was determined using X-tile software. The two-sided log-rank test was used to compare overall survival between high- and low-RAMP1 expression groups. (G) Receiver operating characteristic (ROC) curve analysis of RAMP1 expression for predicting lymph node metastasis in HNSCC patients (n = 77). The area under the curve (AUC) was 0.808 (95% CI: 0.699–0.917). The DeLong method was performed to compare AUCs. *$p < 0.05$, **$p < 0.01$, ***$p < 0.001$.

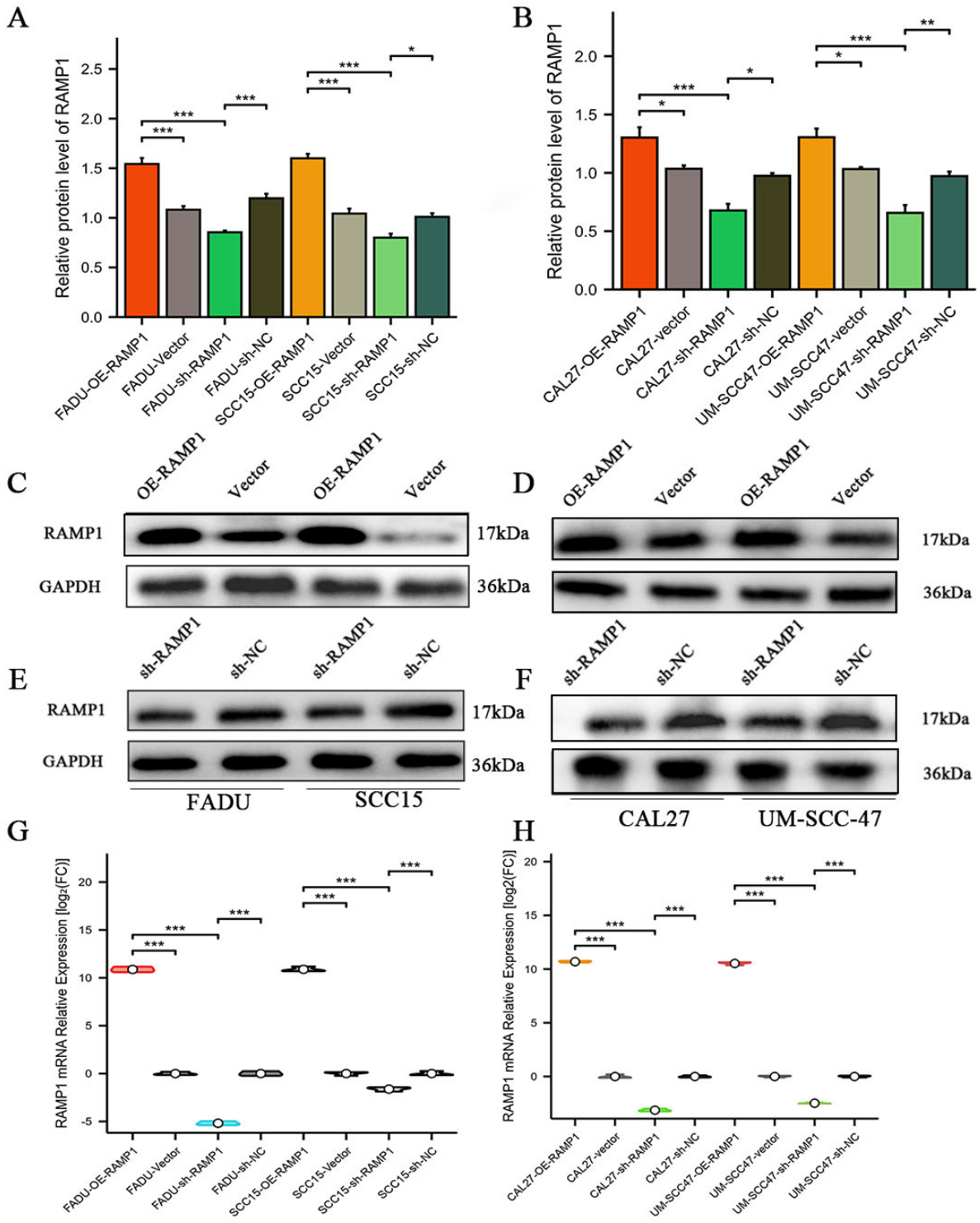

Fig. 5. Successful establishment of stable RAMP1 KD and OE models in HNSCC cell lines. (A,B) Quantification of RAMP1 protein levels in FADU, SCC15, CAL27, and UM-SCC47 cell lines. (C–F) Representative Western blots of RAMP1 levels in FADU, SCC15, CAL27, and UM-SCC47 cells after lentiviral transduction with a non-targeting control shRNA (sh-NC), shRNA targeting RAMP1 (sh-RAMP1), an empty vector control (Vector), or a RAMP1 OE construct (OE-RAMP1). (G,H) qRT-PCR measurement of relative RAMP1 mRNA levels in specified HNSCC cells with stable KD (sh-RAMP1, *vs*. sh-NC control) or OE (OE-RAMP1, *vs*. Vector control). Data are depicted as mean ± SD of at least three separate experiments. Comparisons were performed via a two-tailed Student's *t*-test. *$p < 0.05$, **$p < 0.01$, ***$p < 0.001$.

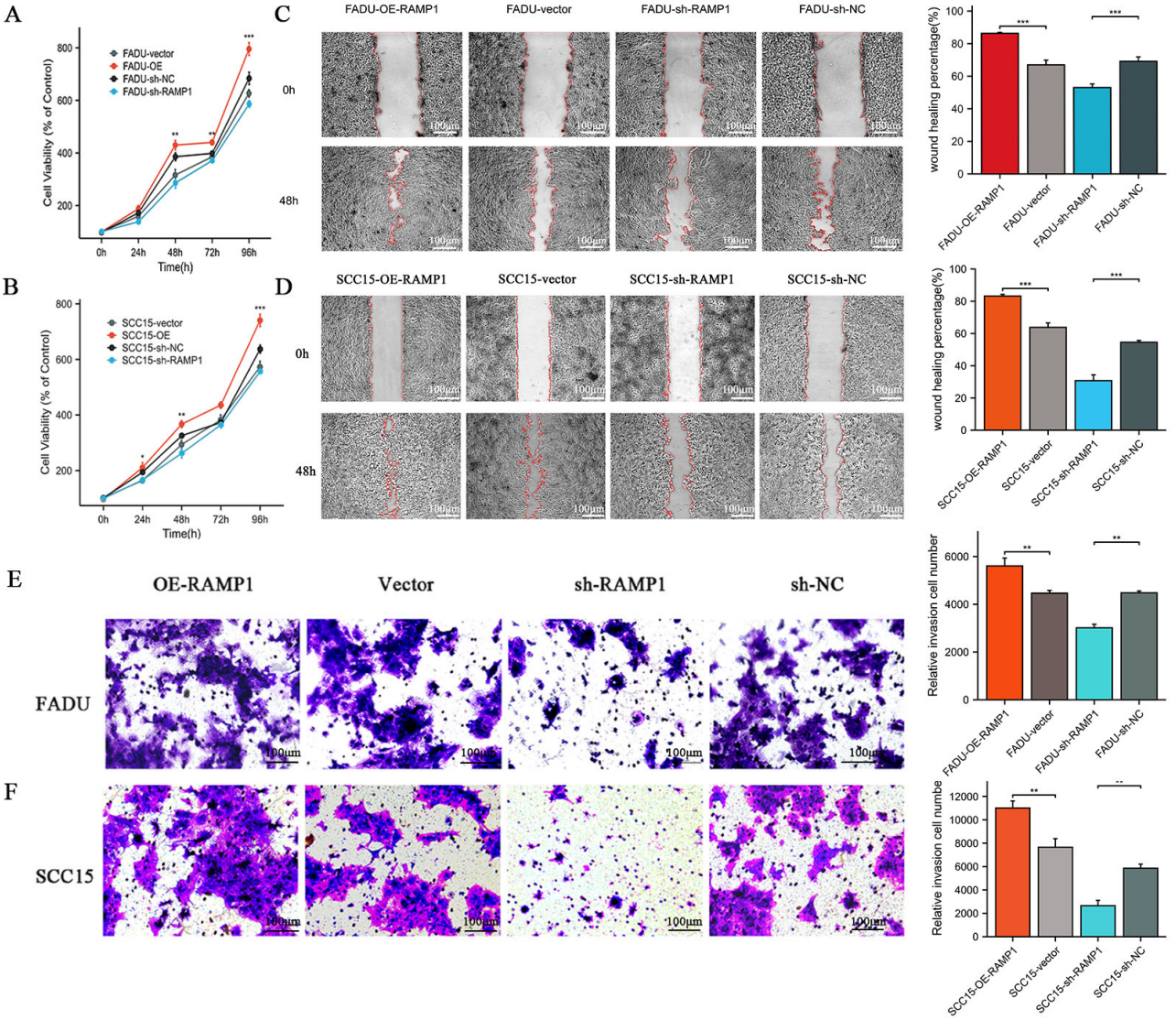

Fig. 6. RAMP1 promotes the proliferation, migration, and invasion of HNSCC cells *in vitro*. The proliferation rates of RAMP1 KD (sh-RAMP1) or OE (OE-RAMP1) in (A) FADU and (B) SCC15 cells were assessed by CCK-8 assay and compared with their respective controls (sh-NC and vector). (C,D) Cell migration was assessed using a wound-healing assay. Representative images and corresponding quantitative analysis of relative wound closure in (C) FADU and (D) SCC15 at 0 h and 48 h. Scale bar, 100 µm. (E,F) Cell invasion ability was determined by the Transwell invasion assay. Representative images (left panel, 200× magnification) and the quantitative analysis of the number of invading. Scale bar: 100 µm. (E) FADU and (F) SCC15 cells (right panel). Data are shown as mean ± SD of three independent experiments. A two-tailed Student's *t*-test was conducted to compare sh-RAMP1 versus sh-NC and OE-RAMP1 versus vector. *$p < 0.05$, **$p < 0.01$, ***$p < 0.001$ *vs*. respective control group.

mary tumor tissues was substantially higher in the LM-positive group relative to the negative group ($p < 0.05$) (Fig. 3C,D). These observations were corroborated through IHC analysis at the tissue level (Fig. 4A,B).

Pan-cancer analysis revealed a broad increase in *RAMP1* expression specifically in HNSCC (Fig. 4C). The TCGA database also confirmed that *RAMP1* expression was substantially increased in the LM-positive group relative to the negative group ($p < 0.05$) (Fig. 4D). Spearman correlations indicated significant positive associations between RAMP1 expression levels and MLVD (r = 0.384, $p < 0.001$) (Fig. 4E), suggesting that RAMP1 can modulate the metastatic process of HNSCC via lymphangiogenesis. Kaplan-Meier curves demonstrated that individuals with high RAMP1 levels had significantly shorter OS relative to those with lower levels (Log-rank $p = 0.041$) (Fig. 4F), suggesting that RAMP1 can function as a prognostic biomarker for HNSCC patients. Receiver operating charac-

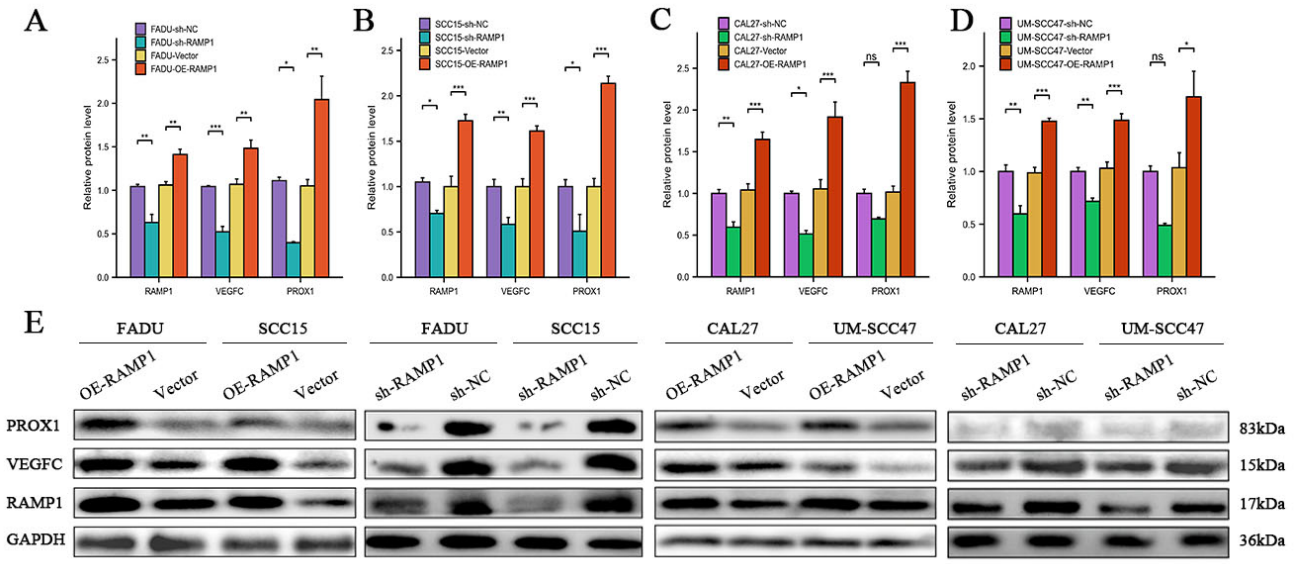

Fig. 7. RAMP1 regulates the expression of key lymphangiogenic factors in HNSCC cells. (A–D) Western blots showing relative levels of RAMP1, VEGF-C, and PROX-1 in (A) FADU, (B) SCC15, (C) CAL27, and (D) UM-SCC47 cells. Protein levels were normalized to GAPDH levels. (E) Western blots showing RAMP1, VEGF-C, and PROX-1 levels in FADU, SCC15, CAL27, and UM-SCC47 cells conditioned to RAMP1 KD (sh-RAMP1) or OE (OE-RAMP1), compared with their respective controls (sh-NC and vector). Data are shown as mean ± SD of at least three independent experiments. Comparisons were performed using two-tailed Student's *t*-tests. **p* < 0.05, ***p* < 0.01, ****p* < 0.001 *vs.* control group. ns, not significant.

teristic (ROC) curve analysis further indicated that RAMP1 expression had good predictive performance for LM, with an area under the curve (AUC) of 0.808 (95% CI: 0.699–0.917) (Fig. 4G).

3.3 RAMP1 Promotes HNSCC Cells' Ability to Proliferate, Migrate, and Invade In Vitro

qRT-PCR and Western blotting indicated that after lentiviral transduction, RAMP1 mRNA and protein levels were substantially reduced in the sh-RAMP1 group relative to the sh-NC group. Moreover, the OE-RAMP1 group had significantly increased levels of RAMP1 mRNA and protein relative to the vector group ($p < 0.05$) (Fig. 5A–H). These findings confirm the successful establishment of stable RAMP1 KD and OE HNSCC cell models. FADU and SCC15 cell lines showed the highest transduction efficiency and represent two major anatomical subsites of HNSCC (hypopharynx and tongue) and were therefore selected for subsequent functional assays.

The CCK-8 proliferation assay showed that RAMP1 KD significantly inhibited the proliferation of FADU and SCC15 cells compared with controls ($p < 0.05$). RAMP1 OE substantially enhanced cell proliferation ($p < 0.05$) (Fig. 6A,B). The wound healing assay revealed that RAMP1 KD significantly decreased FADU and SCC15 cells' migratory capacity ($p < 0.05$), while RAMP1 OE had the opposite effect ($p < 0.05$) (Fig. 6C,D). The Transwell invasion assay showed that RAMP1 KD significantly reduced the number of invading FADU and SCC15 cells ($p < 0.05$), whereas RAMP1 OE showed a reverse trend ($p < 0.05$) (Fig. 6E,F). These data suggest that RAMP1 can elevate the migration, invasion, and proliferation of HNSCC cells.

3.4 RAMP1 Increases the Release of Lymphangiogenic Factors and Endothelial Cell Tube Formation In Vitro

Western blotting revealed that in FADU, SCC15, CAL27, and UM-SCC47 cells, RAMP1 KD significantly reduced VEGF-C and PROX-1 protein expression, while RAMP1 OE significantly up-regulated them ($p < 0.05$) (Fig. 7A–E). These data suggest that RAMP1 can modulate the expression of crucial lymphangiogenic factors, specifically VEGF-C and PROX-1, in HNSCC cells.

The tube formation assay indicated that, compared to the control group, HLECs cultured in medium conditioned by sh-RAMP1 HNSCC cells had sparse, incomplete tubular formations. This treatment significantly decreased the junction count and the overall tube length ($p < 0.05$). HLECs conditioned in OE-RAMP1 cells' medium formed denser, more intricate network structures, with a substantially elevated number of junctions and the total tube length ($p < 0.05$) (Fig. 8A–C). These findings suggest that RAMP1 can promote the tube-forming capacity of lymphatic endothelial cells in a paracrine manner, thus modulating lymphangiogenesis.

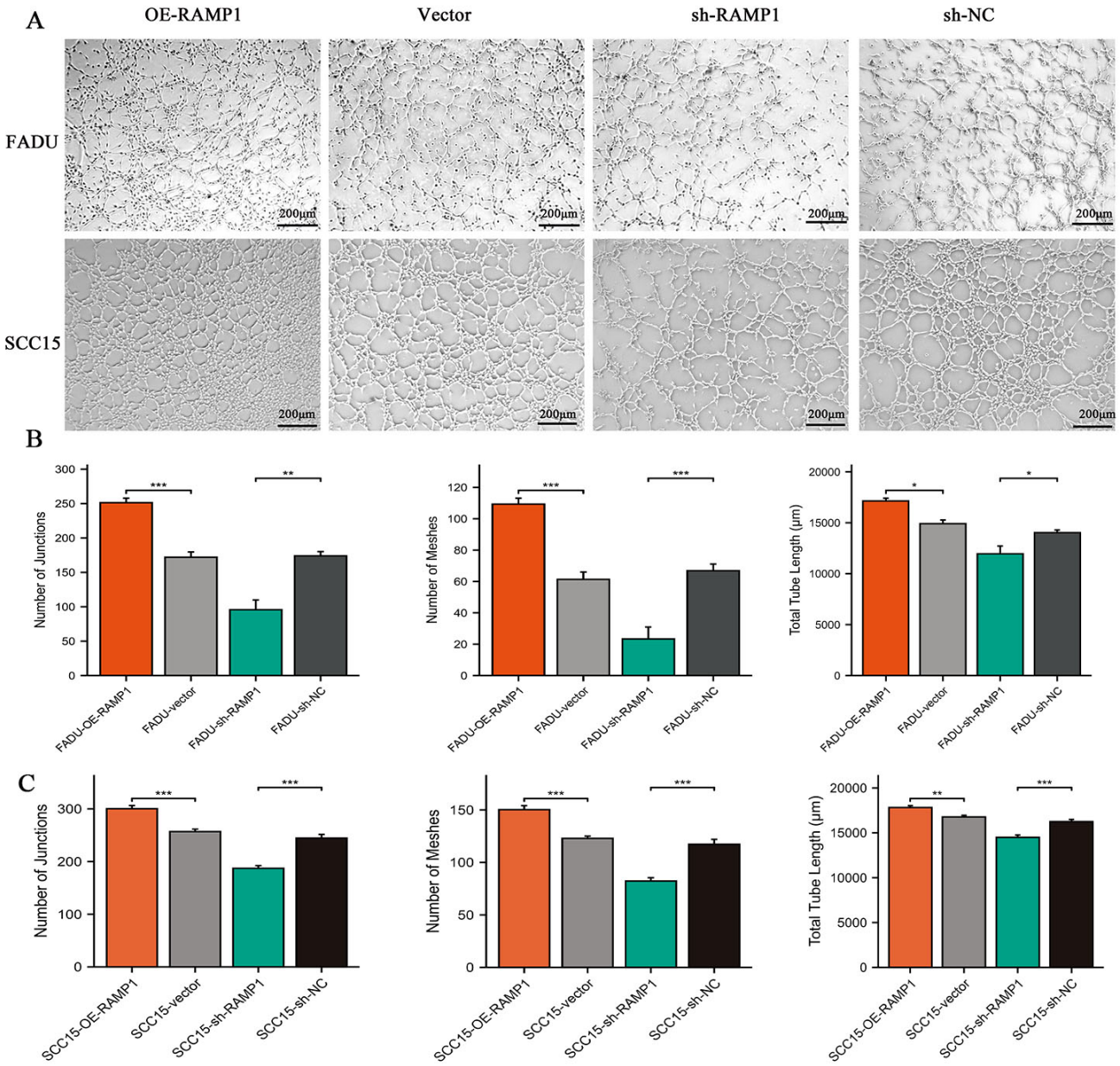

Fig. 8. RAMP1 promotes tube formation in HLECs, an human lymphatic endothelial cell line, *in vitro*. (A) Representative microscopic images of tube formation in HLECs cultured in conditioned medium (CM) from FADU (upper panel) or SCC15 (lower panel) cells with RAMP1 KD (sh-RAMP1) or OE (OE-RAMP1), as well as their respective controls (sh-NC and vector). HLECs were seeded on Matrigel and imaged after 24 hours. Magnification = 10×. Scale bar, 200 μm. (B,C) Quantitative analysis of the tube formation assay for HLECs conditioned to engineered FADU (B) or SCC15 (C) cells. ImageJ software was employed to quantify key parameters, including the number of junctions, meshes, and total tube length. Data are shown as mean ± SD of three separate experiments (with multiple fields analyzed per replicate). For each comparison, a two-tailed Student's *t*-test was performed. *$p < 0.05$, **$p < 0.01$, ***$p < 0.001$ *vs*. control group.

3.5 RAMP1 Promotes In Vivo Tumor Growth and Lymphatic Metastasis in HNSCC

The nude mouse footpad xenograft model indicated that relative to the control group, The OE-RAMP1 group showed a tendency toward increased tumor volume and weight, but the differences did not reach statistical significance (ns, $p \geq 0.05$), while they were significantly decreased in the sh-RAMP1 group ($p < 0.05$) (Fig. 9A–C). Furthermore, IHC analysis confirmed that RAMP1 expression was significantly elevated in tumor tissues from the OE-RAMP1 group but significantly reduced in the sh-RAMP1 group (Fig. 9D). The Western blot analysis indicated that, compared with the control group, the sh-RAMP1 group showed a significant reduction in VEGF-

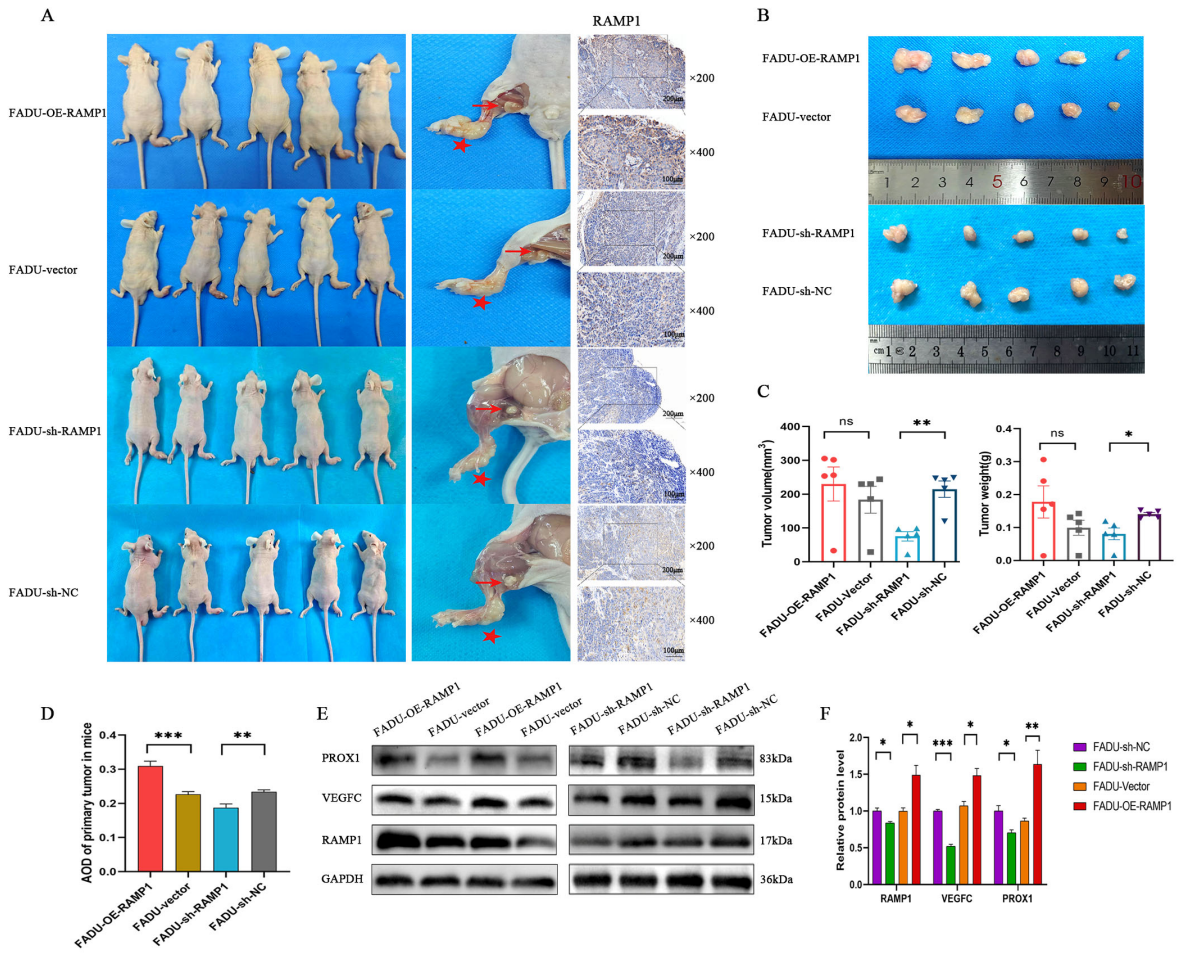

Fig. 9. RAMP1 promotes tumor growth and lymphangiogenesis *in vivo* by up-regulating VEGF-C and PROX-1. (A) Representative images of orthotopic tumors in the footpads of nude mice at the endpoint (day 28). From top to bottom: mice are arranged in the order of FADU-OE-RAMP1, FADU-vector, FADU-sh-RAMP1, and FADU-sh-NC groups. The middle panel shows a detailed anatomical view of a dissected footpad tumor and the popliteal lymph node. The right panel shows representative IHC images of RAMP1 expression in primary tumor tissues. Scale bar: 200 μm (200×) and 100 μm (400×), respectively. (B) Excised primary tumors from the footpads of each group. (C) Quantification of primary tumor volumes (left) and weights (right). (D) Quantification of IHC staining intensity of RAMP1, presented as the Average Optical Density (AOD), which integrates both staining intensity and positive area. (E) Western blots showing RAMP1, VEGF-C, and PROX-1 levels in lysates from primary tumors of FADU-OE-RAMP1 *vs*. FADU-vector or FADU-sh-RAMP1 *vs*. FADU-sh-NC injected mice. (F) Quantification of relative protein levels from (E). Protein expression was normalized to GAPDH. Data are shown as mean ± SD (n = 5). For comparisons between two groups (OE-RAMP1 *vs*. vector; sh-RAMP1 *vs*. sh-NC), a two-tailed Student's *t*-test was conducted. *$p < 0.05$, **$p < 0.01$, ***$p < 0.001$ *vs*. respective control groups. ns, not significant.

C and PROX-1 protein expression in tumor tissues ($p < 0.05$), while they were significantly up-regulated in the OE-RAMP1 group ($p < 0.05$) (Fig. 9E,F), suggesting that RAMP1 can modulate VEGF-C and PROX-1 expression *in vivo*. The IHC analysis via LYVE-1 staining showed that the MLVD in tumor tissues from the sh-RAMP1 group was significantly reduced compared with controls ($p < 0.05$). Moreover, the MLVD in the OE-RAMP1 group was significantly higher than in the control group ($p < 0.05$) (Fig. 10A,B).

The popliteal lymph node analysis revealed that both the volumes and masses of metastatic lymph nodes in the OE-RAMP1 group were significantly higher than in the controls ($p < 0.05$), but the sh-RAMP1 group had substantially reduced sizes and masses ($p < 0.05$) (Fig. 10C–E). Furthermore, IHC analyses revealed that the incidence of LM in the OE-RAMP1 cohort (42.86%) was significantly higher than in the vector cohort (16.67%) and the sh-RAMP1 cohort (0%) (Fig. 10F and Table 3, Ref. [28,29]). These results demonstrate that RAMP1 promotes tumor growth and lymphatic metastasis in HNSCC *in vivo*.

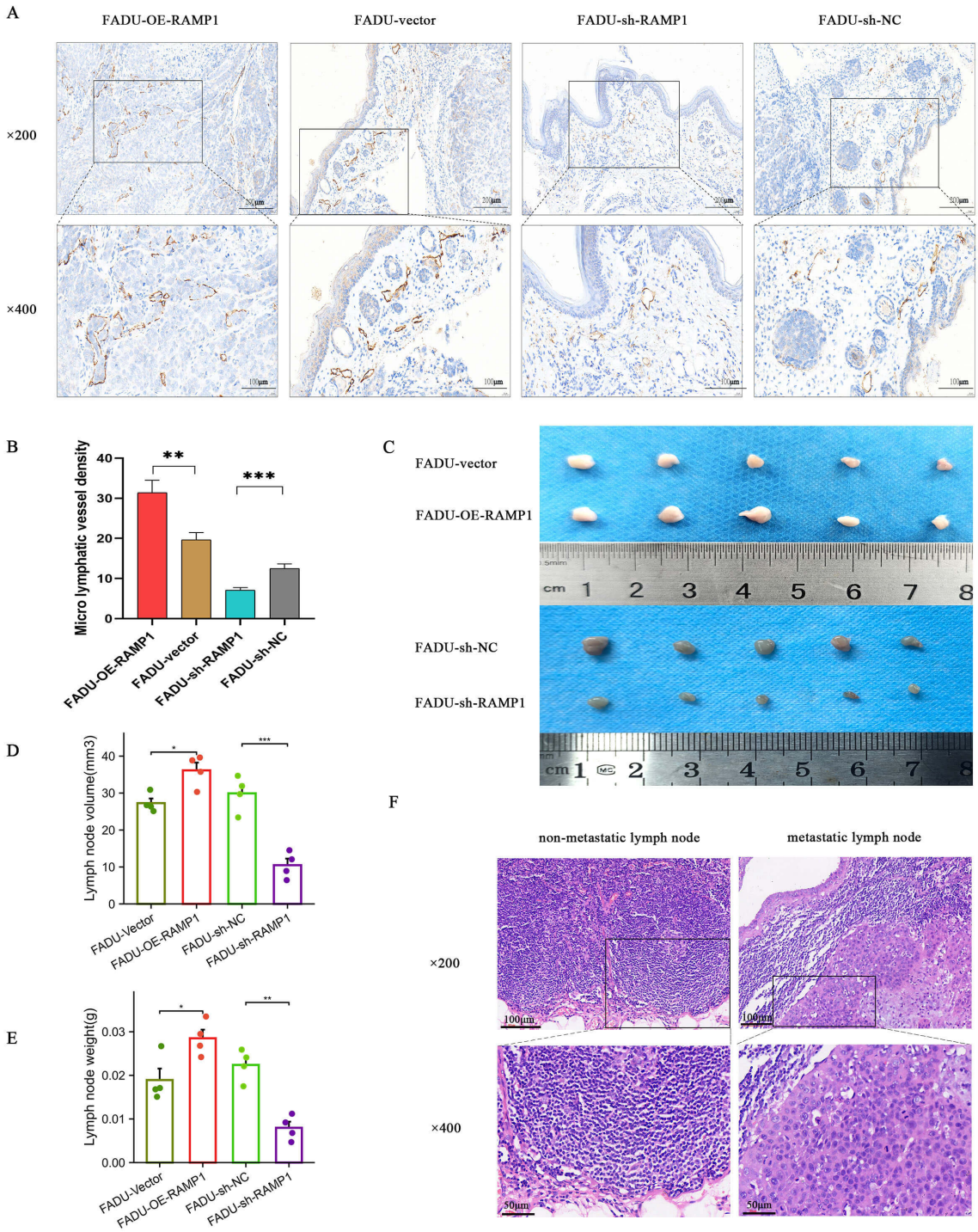

Fig. 10. RAMP1 enhances lymphangiogenesis and promotes LM *in vivo*. (A) Representative IHC images of LYVE-1 (a specific marker for lymphatic endothelial cells) stained tumor sections to visualize intratumoral lymphatic vessels. Scale bar: 200 μm (200×) and 100 μm (400×), respectively. (B) Quantification of MLVD based on LYVE-1-positive vessels in primary tumors from each group. (C) Representative images of lymph nodes collected from nude mice in the indicated groups. (D,E) Quantification of (D) lymph node volumes and (E) weights. (F) Representative H&E staining of lymph nodes, indicating the histology of non-metastatic (left panel) and metastatic (right panel) LNs. For comparisons between two groups (OE-RAMP1 *vs.* vector; sh-RAMP1 *vs.* sh-NC), a two-tailed Student's *t*-test was carried out. Scale bar: 100 μm (200×) and 50 μm (400×), respectively. *$p < 0.05$, **$p < 0.01$, ***$p < 0.001$ *vs.* respective control groups.

Table 3. Incidence of LM in the experimental lymph metastasis model.

Group	Total LNs collected (n)	Metastatic LNs (n)	Metastasis rate (%)	*p*-value
FADU-OE-RAMP1	7	3	42.86	0.045
FADU-vector	6	1	16.67	
FADU-sh-RAMP1	5	0	0	1.000
FADU-sh-NC	5	0	0	

To reliably detect differences in lymph node metastasis rate, the sample size was 5 mice per group, based on previous HNSCC footpad metastasis studies [28,29]. Popliteal lymph nodes were harvested from the right hind footpad. Consistent with tumor-induced lymphangiogenesis and local lymphatic remodeling, some mice exhibited multiple (2–3) lymph nodes within the popliteal fossa, resulting in variation in the total number of lymph nodes collected per group. No mice were excluded from analysis due to this variation. Metastasis rates were calculated as the proportion of metastatic lymph nodes among the total number of collected lymph nodes. Statistical analysis was performed using Fisher's exact test based on 2 × 2 contingency tables (metastatic *vs*. non-metastatic lymph nodes). A significant difference was observed between the OE-RAMP1 and vector groups (*$p = 0.045$). No significant difference was detected between the sh-RAMP1 and sh-NC groups ($p = 1.000$). LNs, lymph nodes.

4. Discussion

The prognosis of HNSCC is influenced by LM incidence, which significantly reduces five-year survival rates [31,32,33]. In LM tumors, lymphangiogenesis is an essential process that provides a structural foundation for tumor cell migration and influences tumor development by modulating the tumor microenvironment and immune responses [34,35]. The mechanism by which the *VEGF-C/VEGFR3* signaling axis activates the transcription factor *PROX-1* to regulate lymphatic endothelial cell phenotype and drive tumor lymphangiogenesis has been comprehensively studied [36,37]; however, the related upstream regulatory mechanisms in HNSCC warrant further research. Therefore, it is crucial to evaluate the upstream regulatory pathway of the *VEGF-C/VEGFR3/PROX-1* axis to identify the mechanisms underlying HNSCC lymphatic metastasis and to develop novel therapeutic strategies.

This systematic study confirmed that *RAMP1* is a novel upstream regulatory factor for lymphangiogenesis and LM in HNSCC. *RAMP1*, a crucial component of the CGRP receptor complex, significantly influences various physiological and pathological processes [38,39]. Previous studies have reported that *RAMP1* promotes tumor progression in prostate cancer via *NKX3.1* [23] and in gastric cancer through the *CGRP–RAMP1* axis [22], and that it contributes to lymphangiogenesis in inflammatory and tissue repair contexts [25,26,27,40]. However, its role in tumor-associated lymphangiogenesis in HNSCC has not been reported, nor has its relationship with the *VEGF-C/PROX-1* signaling axis been defined. To identify essential genes responsible for lymphatic metastasis in HNSCC, transcriptomic sequencing of tumor samples with and without LM was performed. *RAMP1* was identified as one of the most elevated DEGs in the metastatic cohort, suggesting a possible role in the lymphatic metastasis of HNSCC. Furthermore, clinical studies have indicated that increased *RAMP1* expression is correlated with poor prognosis and enhanced intratumoral MLVD in individuals with HNSCC. This suggests that *RAMP1* may serve as a predictive biomarker for HNSCC and modulate lymphangiogenesis.

In vitro functional assays revealed that *RAMP1* significantly increased proliferation, migration, and invasion in HNSCC cells, consistent with its tumor-promoting role in other malignancies [23,24]. This study is the first to show that *RAMP1* not only regulates the malignant behavior of tumor cells but also remodels the tumor microenvironment, specifically by promoting lymphangiogenesis. Furthermore, altering *RAMP1* expression markedly affects *VEGF-C* levels and its downstream transcription factor, *PROX-1*. These findings indicate that *RAMP1* is the upstream regulator of the classic *VEGF-C/VEGFR3/PROX-1* signaling axis, providing a novel understanding of the atypical activation of this pathway in HNSCC. Previous research predominantly focused on the regulation of *VEGF-C* or its downstream effects, whereas this study established that *RAMP1* may serve as a significant upstream regulator, facilitating activation of the *VEGF-C/VEGFR3/PROX-1* signaling pathway. Although the data of this investigation demonstrated that *RAMP1* positively regulates *VEGF-C* and *PROX-1* expression, the precise molecular mechanism remains elusive. However, given that *RAMP1* is a known co-receptor for CGRP and activates *MAPK* and *PI3K* signaling in other tumor types [22,23], it was inferred that *RAMP1* may promote *VEGF-C* transcription via these pathways in HNSCC. In the future, we will perform rescue experiments, including re-expressing *VEGF-C* or *PROX-1* in RAMP1-KD cells, to assess whether these factors are necessary and sufficient for *RAMP1*'s pro-lymphangiogenic effects. Furthermore, complementary approaches such as ChIP and promoter luciferase reporters will be employed to identify the transcriptional hierarchy.

Functional experiments further validated this molecular-level regulation. The tube formation assays revealed that *RAMP1* enhances the tube-forming capacity

of lymphatic endothelial cells in a paracrine manner, consistent with *RAMP1*'s stimulation of lymphangiogenesis observed by Tsuru et al. [40]. This study also validated *RAMP1*'s stimulation of lymphangiogenesis in HNSCC and identified that its molecular mechanism depends on the *VEGF-C/PROX-1* axis. *In vivo* analyses further confirmed that *RAMP1* OE could increase intratumoral lymphatic vessel density by up-regulating *VEGF-C/PROX-1* expression, thus increasing the LM rate. This establishes the complete regulatory pathway of "*RAMP1* - *VEGF-C/PROX-1* - Lymphangiogenesis - LM", offering a novel understanding of the molecular mechanism underlying lymphatic metastasis in HNSCC. Recent literature highlights that lymphatic arteries are not only passive channels for tumor cell migration but can actively recruit tumor cells by secreting chemokines [41]. It was inferred that HNSCC cells can form a lymphatic network conducive to metastasis by increasing *RAMP1* expression, furnishing novel insights into the "active" function of lymphatic vessels during tumor metastasis.

5. Limitations and Future Perspectives

Several limitations of this study should be acknowledged. (1) The size of the clinical cohort was modest, and samples were collected from a single institution. (2) The xenograft model, while informative, lacks a functional immune system. (3) A small number of animals per group were utilized. (4) *VEGF-C* and *PROX-1* were primarily focused, and other lymphangiogenic factors (e.g., *VEGF-D*) were not evaluated, nor was a preclinical evaluation of *RAMP1*-targeted interventions performed.

In the future, larger, multi-center cohorts are needed to validate the prognostic value of *RAMP1*, and immunocompetent mouse models (e.g., conditional knockout) should be used to assess its role in the intact tumor-immune microenvironment. Further studies should determine the precise molecular events linking *RAMP1* to *VEGF-C* and *PROX-1* and explore crosstalk with other lymphangiogenic pathways. At the cellular level, single-cell and spatial transcriptomic analyses should be carried out to help elucidate the heterogeneity and spatial localization of *RAMP1*-expressing cells within the tumor microenvironment. From a translational perspective, RAMP1 is a druggable GPCR-associated protein. The presented findings open the possibility of repurposing existing CGRP receptor antagonists or developing novel *RAMP1*-targeted agents for HNSCC therapy. However, the therapeutic potential of *RAMP1* inhibition warrants evaluation in preclinical models.

6. Conclusions

This study identified *RAMP1* as a critical driver of lymphangiogenesis and lymphatic metastasis in HNSCC. Mechanistically, *RAMP1* promotes the expression of *VEGF-C* and its downstream transcription factor *PROX-1*, thus enhancing tumor cell aggressiveness and paracrine activation of lymphatic endothelial cells. Clinically, elevated *RAMP1* expression correlates with increased intratumoral lymphatic vessel density and poor patient survival, supporting its potential as a prognostic biomarker. These findings validate the *RAMP1/VEGF-C/PROX-1* axis as a previously unrecognized signaling cascade in HNSCC metastasis and suggest that targeting *RAMP1* may represent a promising therapeutic strategy.

Availability of Data and Materials

The raw data and datasets used and analyzed during the current study are available from the corresponding author on reasonable request.

Author Contributions

XL: data curation (equal), software (equal), validation (equal), writing original draft (equal). YL: resources (equal), software (equal), validation (equal). TW: methodology (supporting), software (supporting). LC: data curation (supporting), software (supporting). HW: data curation (supporting), formal analysis (supporting). TL: methodology (supporting), software (supporting). ZW and CL: methodology (supporting), formal analysis (supporting). MinW: methodology (supporting), software (supporting). MengW: methodology (supporting). ZC: methodology (supporting). MP: study design (equal), resources (supporting), supervision (supporting). GH: conceptualization (equal), funding acquisition (equal), resources (equal), supervision (equal). All authors contributed to editorial changes in the manuscript. All authors read and approved the final manuscript. All authors have participated sufficiently in the work and agreed to be accountable for all aspects of the work.

Ethics Approval and Consent to Participate

The study was carried out in accordance with the guidelines of the Declaration of Helsinki. A written consent was signed by the patients or their families/legal guardians. The study was approved by the ethics committee of the Chongqing University Fuling Hospital (No.CQUFH-EC-2025-017) and the Ethics Committee for Experimental Animal Welfare of Chongqing University (No.CQU-IACUC-2025-024). The study was carried out in accordance with the ARRIVE guidelines, the UK Animals (Scientific Procedures) Act, and the National Institutes of Health (NIH) guidelines.

Acknowledgment

We gratefully acknowledge the assistance and instruction from Professor Yue Li of the Department of Pathology, Chongqing University Fuling Hospital.

Funding

This research was funded by Chongqing Fuling Joint Science and Health Medical Research Project Fund (No. 2023KWLH002); National Natural Science Foundation of China (General Program, No. 82373040; Young Scientists Fund, No. 82303447, 82403600).

Conflicts of Interest

The authors declare no conflicts of interest.

Declaration of AI and AI-Assisted Technologies in the Writing Process

During the preparation of this work the authors used DeepSeek in order to check spelling and grammar. After using this tool, the authors reviewed and edited the content as needed and take full responsibility for the content of the publication.

Supplementary Material

Supplementary material associated with this article can be found, in the online version, at https://doi.org/10.31083/FBL49650.

References

[1] GBD 2023 Cancer Collaborators. The global, regional, and national burden of cancer, 1990-2023, with forecasts to 2050: a systematic analysis for the Global Burden of Disease Study 2023. Lancet (London, England). 2025; 406: 1565–1586. https://doi.org/10.1016/S0140-6736(25)01635-6

[2] Moumoulidis PT, Pavlopoulou A, Ünal R, Mavragani I, Georgakilas AG, Kyrodimos E. Nodal tumor volume as a prognostic factor for head and neck squamous cell carcinoma: a systematic review. Frontiers in Bioscience (Landmark Edition). 2021; 26: 235–245. https://doi.org/10.52586/4937

[3] Chi H, Peng G, Song G, Zhang J, Xie X, Yang J, et al. Deciphering a Prognostic Signature Based on Soluble Mediators Defines the Immune Landscape and Predicts Prognosis in HNSCC. Frontiers in Bioscience (Landmark Edition). 2024; 29: 130. https://doi.org/10.31083/j.fbl2903130

[4] Amit M, Liu C, Gleber-Netto FO, Kini S, Tam S, Benov A, et al. Inclusion of extranodal extension in the lymph node classification of cutaneous squamous cell carcinoma of the head and neck. Cancer. 2021; 127: 1238–1245. https://doi.org/10.1002/cncr.33373

[5] Lu T, Li Y, Pan M, Yu D, Wang Z, Liu C, et al. TBC1D14 inhibits autophagy to suppress lymph node metastasis in head and neck squamous cell carcinoma by downregulating macrophage erythroblast attacher. International Journal of Biological Sciences. 2022; 18: 1795–1812. https://doi.org/10.7150/ijbs.68992

[6] Gül O, Erdivanlı ÖÇ, Birinci M, Terzi S, Çeliker M, Okçu O, et al. Impact of Tumor Budding in Head and Neck Cancers on Neck Lymph Node Metastasis and Prognosis. Journal of Clinical Medicine. 2025; 14: 5224. https://doi.org/10.3390/jcm14155224

[7] Jafree DJ, Long DA, Scambler PJ, Ruhrberg C. Mechanisms and cell lineages in lymphatic vascular development. Angiogenesis. 2021; 24: 271–288. https://doi.org/10.1007/s10456-021-09784-8

[8] Zheng H, An M, Luo Y, Diao X, Zhong W, Pang M, et al. PDGFRα^{+}ITGA11^{+} fibroblasts foster early-stage cancer lymphovascular invasion and lymphatic metastasis via ITGA11-SELE interplay. Cancer Cell. 2024; 42: 682–700.e12. https://doi.org/10.1016/j.ccell.2024.02.002

[9] Vaahtomeri K, Alitalo K. Lymphatic Vessels in Tumor Dissemination versus Immunotherapy. Cancer Research. 2020; 80: 3463–3465. https://doi.org/10.1158/0008-5472.CAN-20-0156

[10] Leong SP, Naxerova K, Keller L, Pantel K, Witte M. Molecular mechanisms of cancer metastasis via the lymphatic versus the blood vessels. Clinical & Experimental Metastasis. 2022; 39: 159–179. https://doi.org/10.1007/s10585-021-10120-z

[11] Yang Y, Cao Y. The impact of VEGF on cancer metastasis and systemic disease. Seminars in Cancer Biology. 2022; 86: 251–261. https://doi.org/10.1016/j.semcancer.2022.03.011

[12] Oliver G, Kipnis J, Randolph GJ, Harvey NL. The Lymphatic Vasculature in the 21st Century: Novel Functional Roles in Homeostasis and Disease. Cell. 2020; 182: 270–296. https://doi.org/10.1016/j.cell.2020.06.039

[13] Cui T, Feng C, Jiang H, Jin Y, Feng J. Inhibition of *PFKFB3* Expression Stimulates Macrophage-Mediated Lymphangiogenesis Post-Acute Myocardial Infarction. Frontiers in Bioscience (Landmark Edition). 2023; 28: 277. https://doi.org/10.31083/j.fbl2811277

[14] Liu P, Zhang R, Han L, Zhang X, Ye Y, Yu W, et al. Vasohibin 2 promotes lymphangiogenesis of lung squamous cell carcinoma through snail-dependent vascular endothelial growth factor-D (VEGF-D) signaling pathway. Annals of Translational Medicine. 2022; 10: 39. https://doi.org/10.21037/atm-21-4865 Erratum in: Annals of Translational Medicine. 2022; 10: 1040. https://doi.org/10.21037/atm-2022-45

[15] Liu P, Ding P, Sun C, Chen S, Lowe S, Meng L, et al. Lymphangiogenesis in gastric cancer: function and mechanism. European Journal of Medical Research. 2023; 28: 405. https://doi.org/10.1186/s40001-023-01298-x

[16] Golestannejad P, Monkaresi M, Zhian Zargaran F, Khosravani M, Asgari P, Mobaraki H, et al. Role of Cancer Associated Fibroblast (CAF) derived miRNAs on head and neck malignancies microenvironment: a systematic review. BMC Cancer. 2025; 25: 582. https://doi.org/10.1186/s12885-025-13965-9

[17] Yin S, Song R, Ma J, Liu C, Wu Z, Cao G, et al. Receptor activity-modifying protein 1 regulates mouse skin fibroblast proliferation via the Gαi3-PKA-CREB-YAP axis. Cell Communication and Signaling : CCS. 2022; 20: 52. https://doi.org/10.1186/s12964-022-00852-0

[18] Yang D, Jacobson A, Meerschaert KA, Sifakis JJ, Wu M, Chen X, et al. Nociceptor neurons direct goblet cells via a CGRP-RAMP1 axis to drive mucus production and gut barrier protection. Cell. 2022; 185: 4190–4205.e25. https://doi.org/10.1016/j.cell.2022.09.024

[19] Zhi X, Wu F, Qian J, Ochiai Y, Lian G, Malagola E, et al. Nociceptive neurons promote gastric tumour progression via a CGRP-RAMP1 axis. Nature. 2025; 640: 802–810. https://doi.org/10.1038/s41586-025-08591-1

[20] Huang T, Su J, Wang X, Shi N, Zhang X, He J, et al. Functional Analysis and Tissue-Specific Expression of Calcitonin and CGRP with RAMP-Modulated Receptors CTR and CLR in Chickens. Animals : an Open Access Journal from MDPI. 2024; 14: 1058. https://doi.org/10.3390/ani14071058

[21] Simms J, Hay DL, Wheatley M, Poyner DR. Characterization of the structure of RAMP1 by mutagenesis and molecular modeling. Biophysical Journal. 2006; 91: 662–669. https://doi.org/10.1529/biophysj.106.084582

[22] Parathan P, Tran K, Neil L, Tan T, Carli ALE, Liao Y, et al. Sensory neuropeptide CGRP and its co-receptor RAMP1 drive tumour cell growth in gastrointestinal cancers. BMJ Oncology. 2025; 4: e000842. https://doi.org/10.1136/bmjonc-2025-000842

[23] Logan M, Anderson PD, Saab ST, Hameed O, Abdulkadir SA.

RAMP1 is a direct NKX3.1 target gene up-regulated in prostate cancer that promotes tumorigenesis. The American Journal of Pathology. 2013; 183: 951–963. https://doi.org/10.1016/j.ajpath.2013.05.021

[24] Dallmayer M, Li J, Ohmura S, Alba Rubio R, Baldauf MC, Hölting TLB, et al. Targeting the CALCB/RAMP1 axis inhibits growth of Ewing sarcoma. Cell Death & Disease. 2019; 10: 116. https://doi.org/10.1038/s41419-019-1372-0

[25] Kurashige C, Hosono K, Matsuda H, Tsujikawa K, Okamoto H, Majima M. Roles of receptor activity-modifying protein 1 in angiogenesis and lymphangiogenesis during skin wound healing in mice. FASEB Journal : Official Publication of the Federation of American Societies for Experimental Biology. 2014; 28: 1237–1247. https://doi.org/10.1096/fj.13-238998

[26] Honda M, Ito Y, Hattori K, Hosono K, Sekiguchi K, Tsujikawa K, et al. Inhibition of receptor activity-modifying protein 1 suppresses the development of endometriosis and the formation of blood and lymphatic vessels. Journal of Cellular and Molecular Medicine. 2020; 24: 11984–11997. https://doi.org/10.1111/jcmm.15823

[27] Hosono K, Yamashita A, Tanabe M, Ito Y, Majima M, Tsujikawa K, et al. Deletion of RAMP1 Signaling Enhances Diet-induced Obesity and Fat Absorption *via* Intestinal Lacteals in Mice. In Vivo (Athens, Greece). 2024; 38: 160–173. https://doi.org/10.21873/invivo.13422

[28] Li Y, Pan M, Lu T, Yu D, Liu C, Wang Z, et al. RAF1 promotes lymphatic metastasis of hypopharyngeal carcinoma via regulating LAGE1: an experimental research. Journal of Translational Medicine. 2022; 20: 255. https://doi.org/10.1186/s12967-022-03468-7

[29] Song K, Li Y, Yang K, Lu T, Wang M, Wang Z, et al. Regulatory Effects of SLC7A2-CPB2 on Lymphangiogenesis: A New Approach to Suppress Lymphatic Metastasis in HNSCC. Cancer Medicine. 2024; 13: e70273. https://doi.org/10.1002/cam4.70273

[30] Giganti F, Stavrinides V, Stabile A, Osinibi E, Orczyk C, Radtke JP, et al. Prostate cancer measurements on serial MRI during active surveillance: it's time to be PRECISE. The British Journal of Radiology. 2020; 93: 20200819. https://doi.org/10.1259/bjr.20200819

[31] Gaudioso P, Borsetto D, Polesel J, Tirelli G, Emanuelli E, Menegaldo A, et al. Blood Markers Predicting Clinically Occult Lymph Node Metastasis in Head and Neck Squamous Cell Carcinoma. ORL; Journal for Oto-rhino-laryngology and its Related Specialties. 2024; 86: 32–40. https://doi.org/10.1159/000534079

[32] Mary Jibi A, Basavaraj V. Study of Podoplanin Expression in Head and Neck Squamous Cell Carcinoma. Iranian Journal of Pathology. 2022; 17: 275–284. https://doi.org/10.30699/IJP.2022.547004.2809

[33] Chen X, Zhang L, Lu H, Tan Y, Li B. Development and validation of a nomogram to predict cervical lymph node metastasis in head and neck squamous cell carcinoma. Frontiers in Oncology. 2024; 13: 1174457. https://doi.org/10.3389/fonc.2023.1174457

[34] Dieterich LC, Tacconi C, Ducoli L, Detmar M. Lymphatic vessels in cancer. Physiological Reviews. 2022; 102: 1837–1879. https://doi.org/10.1152/physrev.00039.2021

[35] Fujimoto N, Dieterich LC. Mechanisms and Clinical Significance of Tumor Lymphatic Invasion. Cells. 2021; 10: 2585. https://doi.org/10.3390/cells10102585

[36] Han F, Simeroth S, Zhu J, Gryniuk I, Pranay A, Chen W, et al. Lymphatic endothelial mTORC1 instructs metabolic and developmental signaling during lymphangiogenesis. Developmental Cell. 2025; 60: 2331–2347.e6. https://doi.org/10.1016/j.devcel.2025.04.012

[37] Gauvrit S, Villasenor A, Strilic B, Kitchen P, Collins MM, Marín-Juez R, et al. HHEX is a transcriptional regulator of the VEGFC/FLT4/PROX1 signaling axis during vascular development. Nature Communications. 2018; 9: 2704. https://doi.org/10.1038/s41467-018-05039-1

[38] Xie L, Xiao W, Fang H, Liu G. RAMP1 as a novel prognostic biomarker in pan-cancer and osteosarcoma. PloS One. 2023; 18: e0292452. https://doi.org/10.1371/journal.pone.0292452

[39] Holm A, Edvinsson JCA, Krause DN, Edvinsson L. RAMP1-dependent hormonal regulation of CGRP and its receptor in the trigeminal ganglion. The Journal of Headache and Pain. 2025; 26: 142. https://doi.org/10.1186/s10194-025-02071-7

[40] Tsuru S, Ito Y, Matsuda H, Hosono K, Inoue T, Nakamoto S, et al. RAMP1 signaling in immune cells regulates inflammation-associated lymphangiogenesis. Laboratory Investigation; a Journal of Technical Methods and Pathology. 2020; 100: 738–750. https://doi.org/10.1038/s41374-019-0364-0

[41] Deng H, Zhang J, Wu F, Wei F, Han W, Xu X, et al. Current Status of Lymphangiogenesis: Molecular Mechanism, Immune Tolerance, and Application Prospect. Cancers. 2023; 15: 1169. https://doi.org/10.3390/cancers15041169